JOURNAL OF NANO- AND ELECTRONIC PHYSICS
Vol. **6** No 2, 02020(6pp) (2014)

ЖУРНАЛ НАНО- ТА ЕЛЕКТРОННОЇ ФІЗИКИ
Том **6** № 2, 02020(6cc) (2014)

Grain Boundaries and Electrical Properties of Thin Films of PbTe-Bi_2Te_3 Solid Solutions

D.M. Freik[1,*], B.S. Dzundza[1], L.Yo. Mezhylovska[1], I.B. Gatala[1], S.I. Mudryy[2]

[1] *Vasyl Stefanyk Precarpathian National University 57, Shevchenko Str., 76018 Ivano-Frankivsk, Ukraine*
[2] *Ivan Franko Lviv National University 1, University Str., 79000 Lviv, Ukraine*

(Received 26 February 2014; revised manuscript received 24 March 2014; published online 20 June 2014)

The structure and electrical properties of thin films based on PbTe-Bi_2Te_3 solid solutions with different composition deposited in vacuum on glass ceramic and mica substrates are studied. It is established that vapor-phase condensate has a mosaic structure formed by the Volmer-Weber mechanism of nucleation and implementation of the processes of nucleation, aggregation and coalescence of nanocrystallites. Based on the electrical model, the thickness h and resistivity ρ_H of grain boundaries are determined. It is shown that with increasing content of Bi_2Te_3 increase in the values of h and ρ_H takes place and the latter is one order of magnitude more than the grain resistance ρ_0.

Keywords: Thin films, Lead Telluride, Solid solutions, Thermoelectric properties.

PACS numbers: 68.37.Hk, 78.66.Hf, 81.15.Ef

1. INTRODUCTION

Lead chalcogenides have a wide application in semiconductor electronics. In particular, lead telluride is an effective thermoelectric material for the medium-temperature region of 500-750 K [1, 2]. Both doped PbTe, as well as solid solutions based on it, and thin-film material considerably extend the limits of practical application [2, 3].

Properties of thin films are defined by the electronic processes at intercrystalline boundaries and the film surface. In connection with this, it is necessary to take into account the scattering at interfaces and grain boundaries, misfit dislocations and other growth defects [3-6]. Localization of charge curriers on the near-surface states and their capture by dangling bonds at the crystallite boundaries lead to the formation near these regions of a space charge, in which charge carrier concentration and mobility can substantially differ from the corresponding volume parameters.

In the present work within the electrical model of resistance we have determined the influence of the grain boundaries on the conductance of thin films based on PbTe-Bi_2Te_2 solid solutions deposited on glass ceramic and mica substrates.

2. EXPERIMENTAL TECHNIQUE

Films for the investigation were obtained by deposition of vapor of synthesized material from PbTe-Bi_2Te_3 solid solutions of the compositions 1.3 and 5 mol. % of Bi_2Te_3 in vacuum on the substrates of fresh cleavages (0001) of mica-muscovite and glass ceramic. Evaporator temperature was equal to T_e = 970 K and substrate temperature – T_s = 470 K. Film thickness was specified by the deposition time in the range of τ = 15-60 s and measured by the microinterferometer MII-4.

Obtained samples were studied by the atomic-force microscopy methods [7]. Surface morphology and its profilograms were determined by the results of the atomic-force investigations of vapor-phase condensates.

Measurement of the electric parameters of the films was performed in air at room temperatures in constant magnetic fields on the developed automated plant which provides measurement of the thermoelectric parameters [8]. The studied sample had four Hall and two current contacts. Silver films were used as the ohmic contacts. Current through the samples was ≈ 1 mA. Magnetic field was directed perpendicular to the films surface at the induction of 1.5 T.

3. FILM STRUCTURE

Investigation results of the surface topology of PbTe-Bi_2Te_3 condensates are shown in Fig. 1, 2 and Table 1, 2. Processing factors of production considerably determine the processes of nucleation and growth of nanocrystallites, which, in turn, specify the surface morphology of the condensates in general. Thus, the processes including nucleation of a new phase in the form of separate pyramidal nanoformations of insignificant size: height 10-15 nm and diameter 30-40 nm, take place on the first stages of deposition for the optimal values of processing factors (T_e = 970 K, T_s = 470 K) for the investigated condensates (Fig. 1, 2; Table 1, 2). In the next aggregation mode, nucleation of new islands stops, and molecules adsorbed on the surface participate in the growth of the already formed structures. In the coalescence mode on the later growth stages, which are realized at significant deposition times ($\tau \approx$ 75 s), coalescence of separate nanostructures takes place. In this case, one can observe the decrease in their density and formation of separate structural "giants" and considerable increase in the surface roughness (see Fig. 1b, Table 1). The latter is especially typical for the condensates obtained on glass ceramic, whose structure is non-uniform (Fig. 1). As for the films on fresh cleavages (0001) of mica-muscovite, their structure is more homogeneous (Fig. 2).

The following nucleation mechanisms are possible at the vapor-phase deposition: Frank Van der Merwe mechanism (formation of a continuous layer of condensate), Stranski-Krastanov mechanism (provides the formation on the initial stages of deposition of the so-called wetting layer with further growth of pyramidal nanostructures

* freik@pu.if.ua

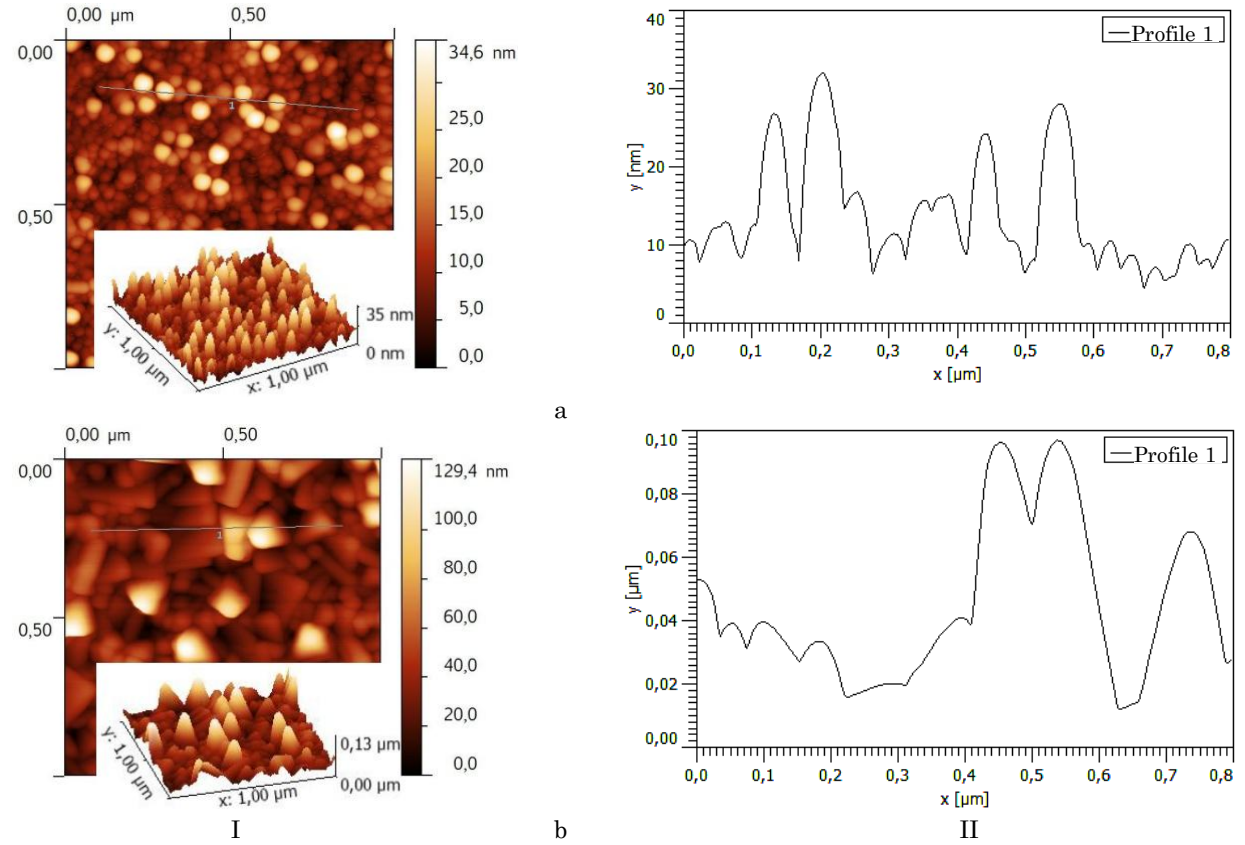

Fig. 1 – AFM-images (I) and profilograms (II) of PbTe + 3 % Bi_2Te_3 films deposited on glass ceramic substrates at deposition times of 15 s (a, No16) and 75 s (b, No13); evaporation temperature T_e = 970 K, substrate temperature T_s = 470 K

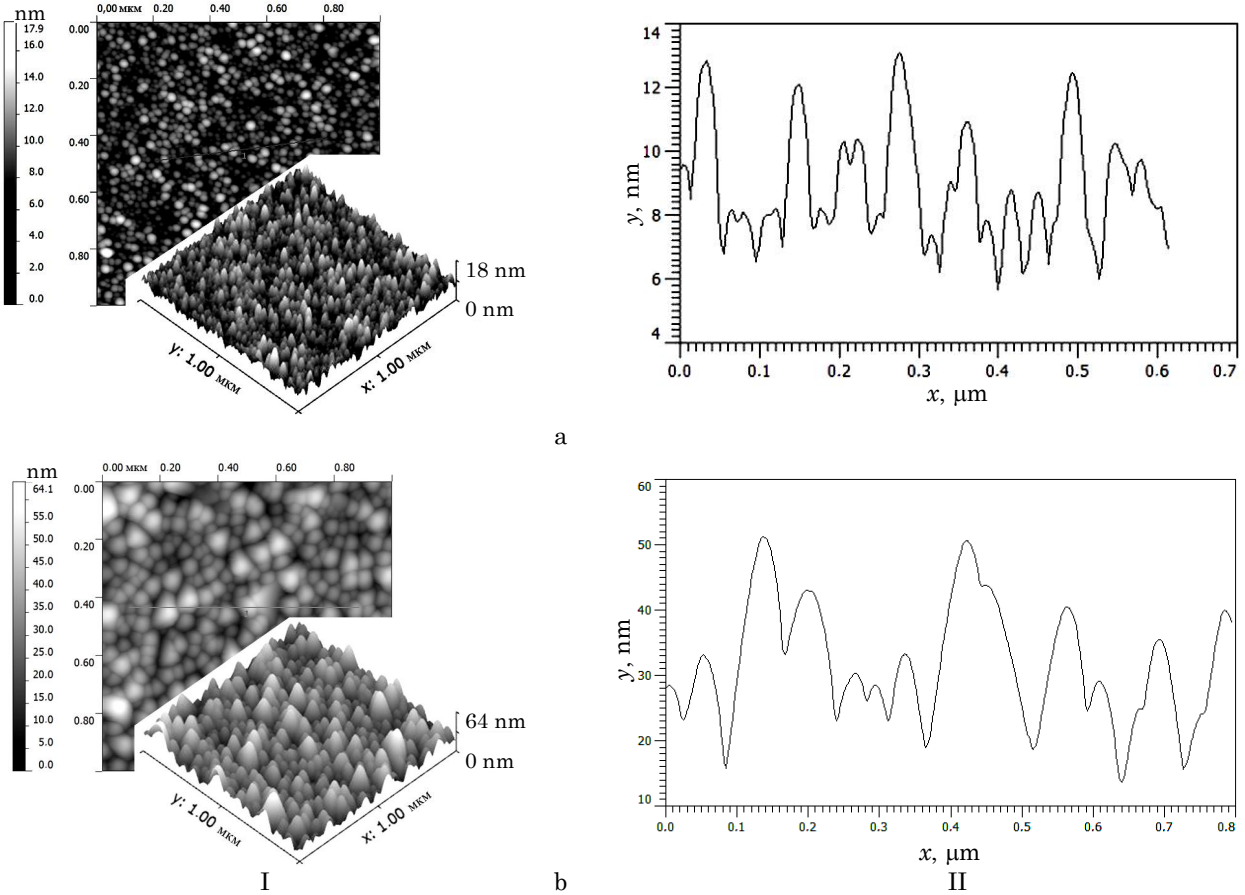

Fig. 2 – AFM-images (I) and profilograms (II) of PbTe + 3 % Bi_2Te_3 films obtained on fresh cleavages (0001) of mica at deposition times of 15 s (a, No2) and 75 s (b, No9); evaporation temperature T_e = 970 K, substrate temperature T_s = 470 K

Table 1 – Structural parameters and processing factors of vapor-phase PbTe-Bi_2Te_3 films on glass ceramic substrates. Evaporation temperature T_e = 970 K, substrate temperature T_s = 470 K

Sample number	Material	Deposition time τ, s	Film thickness d, nm	l, nm	l_1, nm
4	PbTe + 5% Bi_2Te_3	15	270	13	31
5	PbTe + 5% Bi_2Te_3	30	405	23	44
6	PbTe + 5% Bi_2Te_3	45	540	34	43
7	PbTe + 5% Bi_2Te_3	60	810	33	56
8	PbTe + 5% Bi_2Te_3	75	1215	36	38
13	PbTe + 3% Bi_2Te_3	75	1215	39	88
14	PbTe + 3% Bi_2Te_3	60	1000	35	78
15	PbTe + 3% Bi_2Te_3	30	270	21	45
16	PbTe + 3% Bi_2Te_3	15	162	12	41
21	PbTe + 1% Bi_2Te_3	75	2025	102	162
22	PbTe + 1% Bi_2Te_3	60	918	34	100
23	PbTe + 1% Bi_2Te_3	30	634	24	63
24	PbTe + 1% Bi_2Te_3	15	405	14	39

Table 2 – Structural parameters and processing factors of vapor-phase PbTe-Bi_2Te_3 films on mica substrates. Evaporation temperature T_e = 970 K, substrate temperature T_s = 470 K

Sample number	Material	Deposition time τ, s	Film thickness d, nm	l, nm	l_1, nm
1	PbTe + 5% Bi_2Te_3	75	1080	28	41
2	PbTe + 5% Bi_2Te_3	60	810	15	40
3	PbTe + 5% Bi_2Te_3	30	540	9	53
9	PbTe + 3% Bi_2Te_3	75	1080	28	50
10	PbTe + 3% Bi_2Te_3	60	405	21	49
11	PbTe + 3% Bi_2Te_3	30	270	13	34
12	PbTe + 3% Bi_2Te_3	15	108	9	25
17	PbTe + 1% Bi_2Te_3	75	1485	31	49
18	PbTe + 1% Bi_2Te_3	60	675	20	39
19	PbTe + 1% Bi_2Te_3	30	270	12	32
20	PbTe + 1% Bi2Te3	15	135	7	30

Note: l, l_1 are the average normal and lateral sizes of nanostructures

due to the removal of elastic deformations) and Volmer-Weber mechanism (formation of three-dimensional separate nuclei of nanostructures on the substrate surface) [9, 10]. In our case, under all deposition conditions of PbTe-Bi_2Te_3 condensates we observe the formation and growth of separate structures of pyramidal shape (see Fig. 1, 2) that indicates the realization of the Volmer-Weber mechanism.

4. ELECTRICAL MODEL OF FILM RESISTANCE

Bearing in mind that the studied condensates have a mosaic structure (Fig. 1, 2), and in the first approximation for simplification of the calculations they can be represented in the form of parallelepipeds of the height l (grain size in the normal to the surface direction) and base $l_1 \times l_1$ (grain size in the lateral to the surface direction) which have grain boundaries of the thickness h (Fig. 3a) [11]. Then linear size of a monoblock grain will be equal to $b_i = l_i - 2h$ and its resistance $R_0 = \rho_0 b_1^{-1}$, where ρ_0 is the crystallite resistivity. Such electric cell will additionally have four resistances $R_{h||}$ of grain boundaries, which are connected parallel, and two resistances $R_{h\perp}$ series-connected to R_0 (Fig. 3b):

$$R_{h21} = \frac{1}{2} R_{h||1} = \rho_h \frac{l_1}{2lh}, \qquad (1)$$

$$R_{h22} = \frac{1}{2} R_{h||2} = \rho_h \frac{l_1}{2b_1 h},$$

$$R_{h1} = 2R_{h\perp} = \rho_h \frac{2h}{bb_1}. \qquad (2)$$

Here ρ_g is the resistivity of the grain boundary region.

Taking into account the equivalent scheme (Fig. 3c), the total resistance of a crystallite with grain boundaries R_e will be determined by the correlation

$$\frac{1}{R_e} = \frac{1}{R_0 + R_{h1}} + \frac{1}{R_{h21}} + \frac{1}{R_{h22}},$$

$$R_e = \frac{(R_0 + R_{h1}) R_{h21} R_{h22}}{R_{h21}R_{h22} + (R_0 + R_{h1})R_{h22} + (R_0 + R_{h1})R_{h21}}. \qquad (3)$$

Knowing resistance of the film electric cell R_e, one can find its equivalent resistivity

$$\rho_e = R_e l \qquad (4)$$

and also estimate the value of grain boundaries ρ_h and its thickness h defining from profilograms of the dependence of the average crystallite sizes in the lateral l_1 and normal l directions, respectively (Table 1, 2).

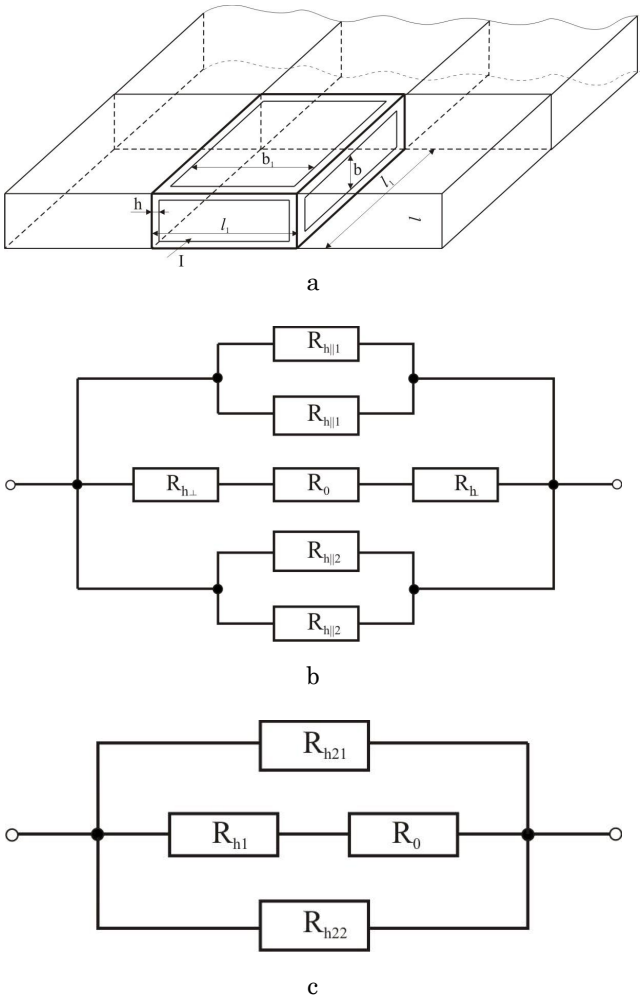

Fig. 3 – Model of a mosaic structure of PbTe films (a) and the equivalent electric schemes (b, c)

5. ELECTRICAL CONDUCTIVITY OF THE FILMS

Thickness dependences of the film resistivity are illustrated in Fig. 4, 5. It is seen that with the increase in the thickness resistivity decreases reaching saturation at thicknesses larger than 1 μm.

Such behavior of the conductivity (Fig. 4, 5) correlates well with the thickness dependence of crystallite sizes (Fig. 1, 2; Table 1, 2) that gives the possibility to assume about the dominant influence of grain boundaries. Taking into account an attainment of saturation by the thickness dependence of the conductivity, the grain resistivity ρ_0 can be defined. Approximating the experimental data by the electric model, the average thickness h and grain boundary resistivity ρ_h are found. The calculation results are represented in Table 3.

We have to note that thickness h and conductivity $\sigma_h = 1/\rho_h$ of grain boundaries increases with increasing content of Bi_2Te_3 in a solid solution (Table 3). Increase in the thickness of grain boundaries can be explained by the decrease in the average crystallite size with increasing Bi_2Te_3 content, i.e. presence of a larger amount of fine crystallites that leads to the increase in the contribution of grain boundaries to the conductivity.

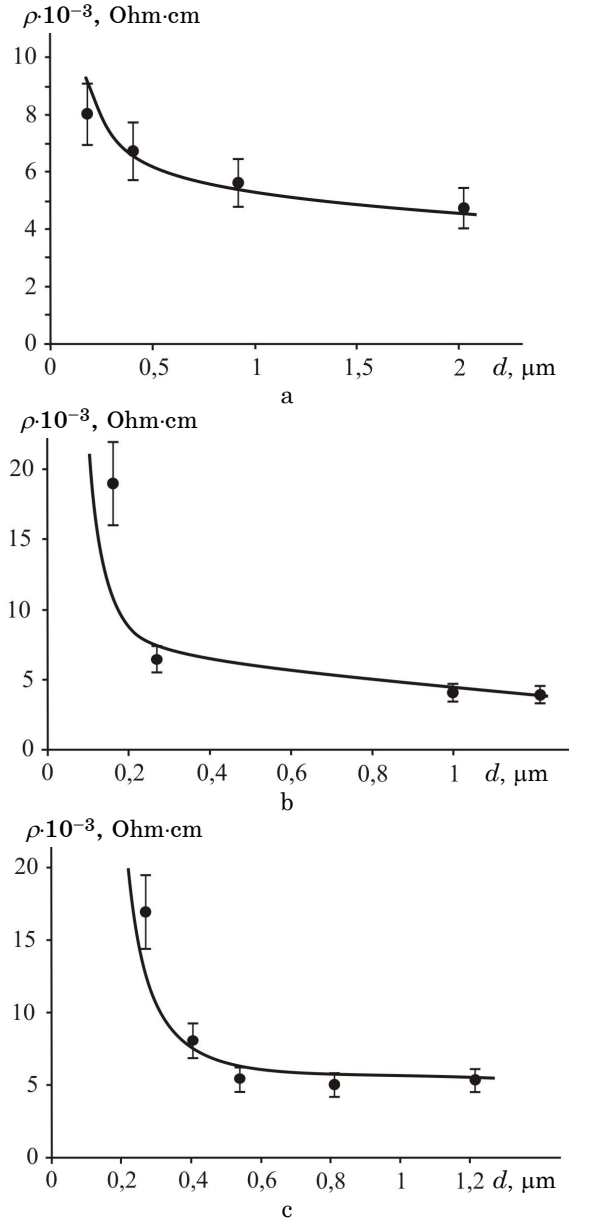

Fig. 4 – Dependence of the resistivity on the thickness for the films: PbTe-(1 mol. %)Bi_2Te_3 (a), PbTe-(3 mol. %)Bi_2Te_3 (b) and PbTe-(5 mol. %)Bi_2Te_3 (c) on glass ceramic substrates. Dots are the experiment; solid lines are the calculation according to the electric model

Calculated resistivity of grain boundaries ρ_h is one order of magnitude larger than the resistance of crystallites ρ_0 (Table 3) that is connected with scattering of charge carriers and diffusion of oxygen along the grain boundaries, which due to the own acceptor action leads to the decrease in the concentration of majority carriers in PbTe-Bi_2Te_3 films of n-type and, therefore, decrease in their electrical conductivity.

Decrease in the resistivity with increasing Bi_2Te_3 content is connected with the increase in the Hall concentration of majority carriers in PbTe-Bi_2Te_3 solid solution that is confirmed by the crystal-chemical calculations [12]. Thus, in particular, bearing in mind that the crystal-chemical formula of nonstoichiometric n-PbTe has the form [12]

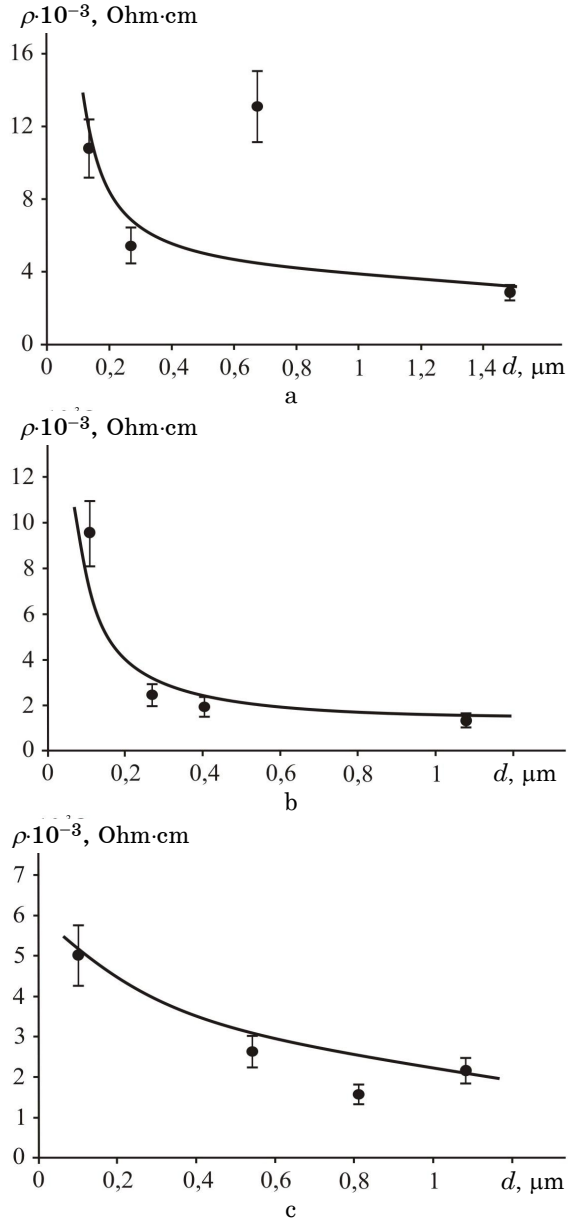

Fig. 5 – Dependence of the resistivity on the thickness for the films: PbTe-(1 mol. %)Bi_2Te_3 (a), PbTe-(3 mol. %)Bi_2Te_3 (b) and PbTe-(5 mol. %)Bi_2Te_3 (c) on fresh cleavages (0001) of mica-muscovite. Dots are the experiment; solid lines are the calculation according to the electric model

$$\left[\mathrm{Pb}^{x}_{1-\alpha\sigma}\,\mathrm{V}^{//}_{\alpha\sigma(1-\delta)}\mathrm{V}^{/}_{\alpha\sigma\delta}\right]_{\mathrm{Pb}}\left[\mathrm{Te}^{x}_{1-\alpha}\mathrm{V}^{\cdot\cdot}_{\alpha}\right]_{Te}\left(\mathrm{Pb}^{\cdot\cdot}_{\alpha\sigma}\right)_i+(2\alpha+\alpha\sigma\delta)e^-$$

and cluster of the doping compound Bi_2Te_3 at the rate of one bismuth atom $Bi^{3+}Te^{2-}_{3/2}$ is equal to

$$\mathrm{V}^{//}_{\mathrm{Pb}}\mathrm{V}^{\cdot\cdot}_{\mathrm{Te}}+\mathrm{Bi}^{\cdot\cdot\cdot}\mathrm{Te}^{//}_{3/2}\rightarrow\mathrm{Bi}^{\cdot}_{\mathrm{Pb}}\mathrm{Te}^{x}_{\mathrm{Te}}\left(\mathrm{Te}^{x}_{1/2}\right)_i+e^-, \qquad (5)$$

then the crystal-chemical formula of n-PbTe-Bi_2Te_3 will be represented as follows:

$$\left[\mathrm{Pb}^{x}_{(1-x)(1-\alpha\sigma)}\mathrm{Bi}^{\cdot}_{x}\mathrm{V}^{//}_{\alpha\sigma(1-\delta)(1-x)}\mathrm{V}^{/}_{\alpha\sigma\delta(1-x)}\right]_{\mathrm{Pb}}\left[\mathrm{Te}^{x}_{(1-\alpha)(1-x)+x}\mathrm{V}^{\cdot\cdot}_{\alpha(1-x)}\right]_{\mathrm{Te}}$$
$$\left(\mathrm{Pb}^{\cdot\cdot}_{\alpha\sigma(1-x)}\right)_i\left(\mathrm{Te}^{x}_{1/2}\right)_i+\left\{(2\alpha+\alpha\sigma\delta)(1-x)+x\right\}e^-. \qquad (6)$$

Table 3 – Calculated parameters of grain boundaries for the films of PbTe-Bi_2Te_3 solid solutions

Material	Substrate	Grain boundary thickness h, nm	Grain resistivity ρ_0, 10^{-3} Ohm cm	Grain boundary resistivity ρ_h, 10^{-2} Ohm cm
PbTe + 1% Bi_2Te_3	Glass ceramic	2.8	3.6	2.0
PbTe + 3% Bi_2Te_3		4.2	1.5	1.8
PbTe + 5% Bi_2Te_3		5.2	1.0	1.5
PbTe + 1% Bi_2Te_3	Mica	2.8	1.0	1.5
PbTe + 3% Bi_2Te_3		4.2	0.5	0.6
PbTe + 5% Bi_2Te_3		4.3	0.4	0.5

Here V_{Pb}, V_{Te} are the vacancies of lead and tellurium; Bi_{Pb}, Te_{Te} are the ions of atoms in the corresponding sublattices; Pb_i, Te_i are the ions in interstices; α is the deviation from stoichiometric composition in the base compound; δ is the coefficient of disproportionation of the charge state; σ is the fraction of interstitial Pb_i ions; x is the composition of solid solution.

Thus, in particular, for n-PbTe-Bi_2Te_3, in accordance with (6), equation of complete electrical neutrality will be defined by the correlation

$$\begin{aligned} n+\left|q_{\mathrm{V}''_{\mathrm{Pb}}}\right|[\mathrm{V}''_{\mathrm{Pb}}]+\left|q_{\mathrm{V}'_{\mathrm{Pb}}}\right|[\mathrm{V}'_{\mathrm{Pb}}]= \\ =p+\left|q_{\mathrm{V}^{\cdot\cdot}_{\mathrm{Te}}}\right|[\mathrm{V}^{\cdot\cdot}_{\mathrm{Te}}]+\left|q_{\mathrm{Pb}_i^{\cdot\cdot}}\right|[\mathrm{Pb}_i^{\cdot\cdot}]+\left|q_{\mathrm{Bi}^{\cdot}_{\mathrm{Pb}}}\right|[\mathrm{Bi}^{\cdot}_{\mathrm{Pb}}], \end{aligned} \qquad (11)$$

where $n=A\left((2\alpha+\alpha\sigma\delta)(1-x)+x\right)$, $[\mathrm{V}''_{\mathrm{Pb}}]=A\left(\alpha\sigma(1-\delta)(1-x)+x/3\right)$, $[\mathrm{V}'_{\mathrm{Pb}}]=A\alpha\sigma\delta(1-x)$, $[\mathrm{Bi}^{\cdot}_{\mathrm{Pb}}]=Ax$, $[\mathrm{V}^{\cdot\cdot}_{\mathrm{Te}}]=A\alpha(1-x)$, $[\mathrm{Pb}_i^{\cdot\cdot}]=A\alpha\sigma(1-x)$, $\left|q_{\mathrm{V}'_{\mathrm{Pb}}}\right|=\left|q_{\mathrm{Bi}^{\cdot}_{\mathrm{Pb}}}\right|=1$, $\left|q_{\mathrm{V}''_{Pb}}\right|=\left|q_{\mathrm{V}^{\cdot\cdot}_{\mathrm{Te}}}\right|=\left|q_{\mathrm{Pb}_i^{\cdot\cdot}}\right|=2$.

Here $A=2z/a^3$, z is the number of structural units in the crystal unit cell, a is the lattice parameter.

Hall concentration of charge carriers n_H will have the following form:

$$n_H=A\left((2\alpha+\alpha\sigma\delta)(1-x)+x\right). \qquad (12)$$

When implementing the mechanism of substitution of lead positions by bismuth (Bi^{+}_{Pb}) with the formation of interstitial tellurium (Te^0_i) in n-PbTe-Bi_2Te_3, the Hall concentration of charge carriers n_H appreciably increases with increasing Bi_2Te_3 content (Fig. 6, curve 1).

According to the presented calculations it is established that ionized bismuth atoms in cation sublattice of lead telluride Bi^{+}_{Pb} (Fig. 6, curve 2) and also vacancies of tellurium V^{2+}_{Te} (Fig. 6, curve 5) give the maximum contribution to the formation of majority carriers. Here we should pay attention to significant growth of concentration Bi^{+}_{Pb} with increasing content of doping impurity Bi_2Te_3 in n-PbTe-Bi_2Te_3 solid solution (Fig. 6, curve 2). As for the other point defects [V^{2-}_{Pb}], [V_{Pb}], [Pb^{2+}_i], their

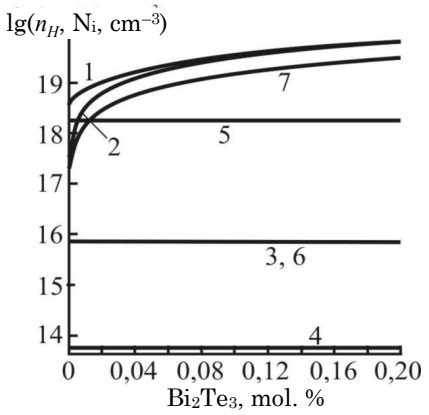

Fig. 6 – Dependence of the concentration of dominant point defects (2-7 - Ni) and Hall concentration of charge carriers (1 – n_H) in n-PbTe-Bi_2Te_3 on the content of Bi_2T_3: 2 – [Bi^{+}_{Pb}]; 3 – [V^{2-}_{Pb}]; 4 – [V_{Pb}]; 5 – [V^{2+}_{Te}]; 6 – [Pb^{2+}_{i}]; 7 – [Te^{0}_{i}]

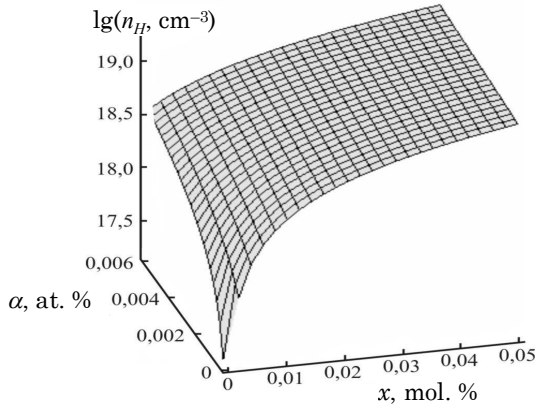

Fig. 6 – Space diagram of the dependence of the Hall concentration of charge carriers (n_H) on the value of nonstoichiometry of PbTe (α) and Bi_2Te_3 content (x) in n-PbTe-Bi_2Te_3 solid solutions

concentration in solid solution is considerably less (Fig. 6, curves 3, 4, 6). Neutrally charged interstitial tellurium Te^{0}_{i}, in spite of its significant concentration (Fig. 6, curve 7), does not change the Hall concentration of carriers.

Dependence of the Hall concentration on the initial deviation from stoichiometry (α) in the principal matrix and Bi_2Te_3 impurity content (x) is well illustrated by the space-diagram n_H-α-x (Fig. 7).

6. CONCLUSIONS

1. We have studied the structure and thermoelectric properties of vapor-phase thin films based on n-PbTe-Bi_2Te_3 solid solutions of different composition obtained on glass ceramic and mica substrates.

2. In the framework of the electrical model of resistance of polycrystalline films we have determined the average thickness and resistivity of grain boundaries.

3. It is shown that the thickness and conductivity of grain boundaries increase with increasing Bi_2Te_3 content in the solid solution.

4. Stable n-type conductivity and high concentration of charge carriers (10^{19}-10^{20} cm^{-3}) are explained by the substitution in n-PbTe-Bi_2Te_3 solid solutions of lead in the principal matrix by bismuth ions ($Bi^{3+} \rightarrow Bi^{1+}_{Pb}$).

AKNOWLEDGEMENTS

This work has been performed under the financial support of the Ministry of Education and Science of Ukraine (Project No 0113U000185) and the State Fund for Fundamental Research of Ukraine (0113U003689) and in the framework of the NATO Program "Science for Peace and Security" (NUKR SFPP984536).

REFERENCES

1. V.M. Shperun, D.M. Freik, R.I. Zapukhlyak, *Termoelektryka telurydu svyntsyu ta yogo analogiv* (Ivano-Frankivsk: Play: 2000).
2. D.M. Freik, M.A. Galushchak, L.Yo. Mezhylovska, *Fizika i tekhnologiya tonkih plenok* (Lviv: Vyshcha shkola: 1988).
3. D.M. Freik, B.S. Dzundza, J.S. Yavorskyy, L.Yo. Mezhylovska, *FKhTT* **14**, No1, 82 (2013).
4. J.N. Zemel, *J. Lumin.* **7**, 524 (1973).
5. *Poverkhnostnye svoystva tverdykh tel* (Pod. red. M. Grina) (M.: Mir: 1972).
6. P.R. Vaya, J. Majht, B.S.V. Gopalam, C. Dattatrepan, *phys. status solidi a* **87**, 341 (1985).
7. D.M. Freik, B.S. Dzundza, J.S. Yavorskyy, et al., *J. Nano-Electron. Phys.* **5** No3, 03054 (2013).
8. M.O. Galushchak, B.S. Dzundza, A.I. Tkachuk, *Metody ta prylady kontrolyu yakosti* **30** No1, 79 (2013).
9. *Nanostrukturirovannye khalkogenidy svintsa: monografiya* (S.P. Zimin, E.S. Gorlachev) (Yaroslavl: YarGU: 2011).
10. S.V. Volkov, E.P. Kovalchuk, V.M. Ogenko, O.V. Reshetnyak, *Nanokhimiya, nanosystemy, nanomaterialy* (K.: Naukova dumka: 2008).
11. Ya.P. Saliy, I.M. Freik, *FKhTT* **5** No1, 94 (2004).
12. D.M. Freik, L.V. Turov, V.V. Boychuk, *Chem. Met. Alloy.* **5**, 77 (2012).